Coupling between Phase Separation and Surface Deformation Modes in Self-Organizing Polymer Blend Films

Brett D. Ermi,[1] Giovanni Nisato,[1] Jack F. Douglas,[1] John A. Rogers,[2] and Alamgir Karim[1]
[1]*Polymers Division, National Institute of Standards and Technology, Gaithersburg, Maryland 20899*
[2]*Bell Laboratories, Lucent Technologies, 600 Mountain Avenue, Murray Hill, New Jersey 07974*
(Received 8 June 1998)

Phase separation of ultrathin polymer blend films spun cast onto patterned self-assembled monolayers is examined by atomic force microscopy. Fourier transform analysis of the time evolution of the film topography reveals a coupling between the phase separation process and the surface deformation modes of the blend film. Excitation of these surface modes occurs when the scales of the phase separation coarsening and the deformation modes become commensurate. These excitations decay with time, leading to a structure where only the fundamental mode has appreciable amplitude. [S0031-9007(98)07518-8]

PACS numbers: 68.15.+e, 61.41.+e, 68.35.Bs, 64.75.+g

The presence of a deformable fluid-air boundary in thin polymer films makes their structure sensitive to instabilities caused by material heterogeneity and thermal fluctuations. Since these perturbations influence the qualitative structure and long term stability of the film, a better understanding of these effects is required if the goal of nanometer level control of surface patterns in biological and materials sciences is to be achieved. Recently, it has been shown that *lateral* phase separation in ultrathin blend films ($L < 200$ nm) results in composition dependent surface morphologies, which "dissolve" when the film is returned to the one phase region [1]. These studies emphasized composition fluctuations which occur in films sufficiently thin to suppress "surface-directed" phase separation [1–3]. Moreover, it has been shown that even the structure of single component polymer films can be sensitive to thermally excited surface undulations ("capillary waves") [4–6]. These observations lead us to consider the existence of a coupling between height and composition fluctuations during phase separation.

Composition fluctuations of phase separation and film height variations are both characterized by continuous dispersion relations associated with the presence of fluctuations occurring over a continuous range of spatial scales [5,7]. Studies of mode coupling between height and composition fluctuations can be facilitated by aligning the coexisting phases of a phase separating blend onto finite regions. In such restricted geometries the surface fluctuations have *discrete* spectra along with allowed symmetries associated with the shape of the confining boundaries. Previous studies have demonstrated "pattern-directed" phase separation of polymer blend films using substrates possessing periodic chemical potential modulations which have a selective affinity for the blend components [8]. The stripe pattern considered in this Letter is a particularly convenient geometry, since the normal modes governing the surface deformations are readily determined and have a quantized form allowing their discrimination from the phase separation process [9].

In this Letter we consider the phase separation of a model blend [deuterated polystyrene (dPS)/polybutadiene (PB)] on a chemically heterogeneous self-assembled monolayer substrate (SAM). Our measurements show a "resonant" coupling between the phase separation process and the surface deformation modes. The quantized surface undulation modes become excited when the average scale of phase separation is commensurate with the scales of the surface modes. The initial phase separation scale is much smaller than the SAM pattern width, yet the influence of the underlying pattern is evident. As the phase separation process develops further, the higher frequency surface modes decay and the lower frequency modes become excited, leading to a final state, where the fundamental mode dominates.

Blend films of dPS ($M_w = 1000$, $M_w/M_n = 1.13$)/PB [10] ($M_w = 5300$, $M_w/M_n = 1.07$) were spun cast from toluene solutions onto SAM covered substrates that were patterned over a 1 cm^2 area surrounded by a homogeneous-COOH terminated SAM region. The pattern consists of alternating ≈ 2 μm lines ("stripes") of -CH_3 and -COOH terminated alkane thiols [$HS(CH_2)_{15}CH_3$ and $HS(CH_2)_{15}COOH$, respectively] prepared using the microcontact printing method [11]. Since the substrate is topographically flat, lateral force microscopy measurements were performed to characterize the substrates, yielding a stripe-patterned periodicity of 4.0 ± 0.1 μm. The dPS/PB blend exhibits an upper critical solution temperature of 51 °C and a critical composition of $\phi_{\mathrm{dPS}} = 0.70$ [12]. For this study 100 and 60 nm films [13] were prepared by spin coating (1000 rpm) from critical composition toluene solutions having total polymer mass fractions of 3% and 2%, respectively. The phase separation kinetics of these viscous films are sufficiently slow such that the morphologies may be considered static relative to the time scale of the measurement. A Topometrix [14] Accurex AFM was used to acquire the topographic and lateral force images to an estimated lateral resolution of ± 25 nm, a vertical resolution of ± 1 nm. The experiments were performed in

 0031-9007/98/81(18)/3900(4)$15.00 © 1998 The American Physical Society

the contact mode using pyramidal Si_3N_4 tips (Topometrix, contact AFM-1520) supplied by the manufacturer. The tip cantilevers had a nominal force constant of 0.032 $\mathrm{N\,m^{-1}}$, and forces applied by the tip to the sample were in the range of 1 to 20 nN. All structures shown in the images were reproducible and independent of scan direction or scan range.

First, we make an initial examination of the influence of the patterned substrate by direct atomic force microscopy (AFM) measurements of the deformation of the polymer-air interface. In Figs. 1(a) and 1(c) we illustrate the topography for a 100 nm thick dPS/PB blend film spun cast on the unpatterned region of the SAM covered substrate (i.e., homogeneous-COOH SAM region), measured after 450 and 3100 min, respectively. Morphologies similar to those in Figs. 1(a) and 1(c) have been observed in our previous studies of phase separation on homogeneous silicon substrates [1,3]. Figures 1(b) and 1(d) correspond to the topography of the same film, but now within the stripe-patterned region after 420 and 3060 min, respectively. In the first measurement intervals [Figs. 1(a) and 1(b)] the observed topography appears homogeneous, but it is evident that the SAM covered substrate strongly influences the coarsening, thereafter such that the developing morphology becomes increasingly aligned with the underlying stripe pattern with time [Fig. 1(d)]. A convenient means for comparing such pattern formation is to average the height profile data transverse to (defined as the x direction) and along (defined as the y direction) the axis parallel to the stripes. The data in Figs. 1(e) and 1(f) display the y-axis averaged topographical height profile plotted along the x direction, $h_y(x) = \langle H(x,y)\rangle_y/\overline{H}$, ($\overline{H}$ is the mean film height) for the data in Figs. 1(c) and 1(d), respectively. As expected for isotropic pattern formation, Fig. 1(e) shows random height fluctuations. We note that the averages along the x direction for both Figs. 1(c) and 1(d) (not shown) are qualitatively identical to Fig. 1(e). In contrast, Fig. 1(f) shows the periodicity and high degree of spatial correlation of the mean average height fluctuations along the y direction. It is clear that the chemical modulation imposed by the substrate directs the observed topography since the qualitative nature of the stripe pattern observed in Fig. 1(d) and the periodicity observed in Fig. 1(f) are equivalent to that of the SAM stripe pattern.

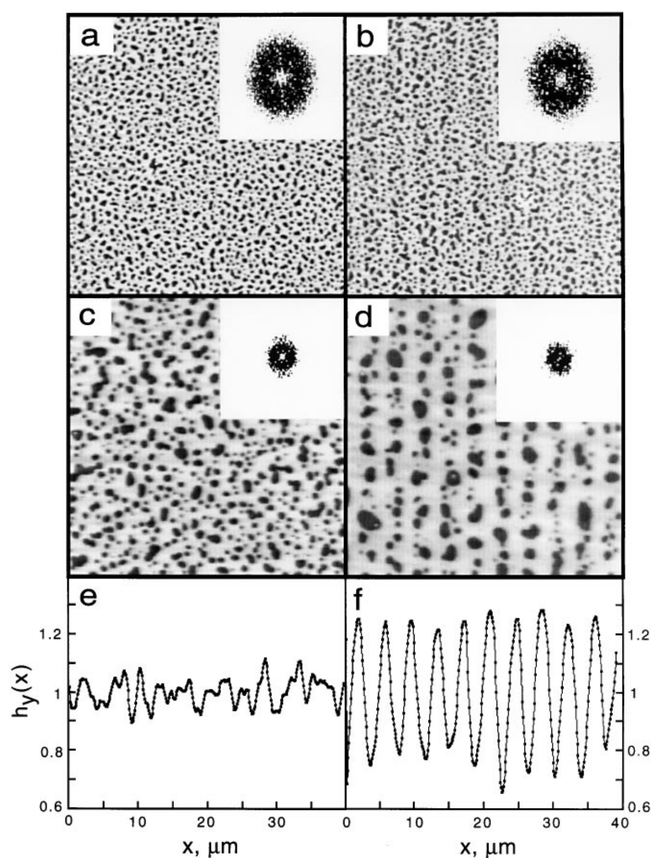

FIG. 1. Comparison of morphology evolution for 100 nm thick dPS/PB film on chemically homogeneous and heterogeneous SAM substrates, with the left-hand side representative of samples on homogeneous substrate and the right-hand side representative of samples on the stripe-patterned substrate. All AFM images are 40 μm × 40 μm with dark regions corresponding to lower features and bright regions corresponding to higher features, measured after (a) 450, (b) 420, (c) 3100, and (d) 3060 min. Insets in (a)–(d) are results of a 2D FFT analysis of the height fluctuations. The averaged height profiles along the y direction for (c) and (d) are shown in (e) and (f), respectively (see text). Instrumental resolution is on the order of symbol size. The periodicity (4 μm) seen in (f) matches that of the SAM pattern.

The insets of Figs. 1(a)–1(d) display the 2D fast Fourier transforms (FFT) of the AFM height profiles. We observe that the scale of the surface structures grows with time. In Fourier space, the same trend is illustrated by the 2D FFT ring shifting towards lower k values, where k denotes the wave vector magnitude. The intensity ring is qualitatively similar in all images, being essentially isotropic for the films on the homogeneous as well as the stripe-patterned substrates, i.e., $k_x^* = k_y^* = k^*$, where k^* is the wave vector at which the FFT amplitude of the diffuse ring is maximum. Correlations along the x axis arising from the imposed stripe pattern do exist in the 2D FFT images, but are difficult to observe because of their sharpness (1–3 pixels in width). As described below, it is possible to separate these "diffraction peaks" from the isotropic ring and analyze these features independently.

Figure 2 displays the radial averaged power spectra, $P(k)$, obtained from the FFT analysis of the height data for 30, 270, and 540 min, respectively, for a 60 nm blend film on a stripe-patterned substrate. This data can be fit adequately with a shifted Lorentzian: $P(k) = A + B/[(k - k^*)^2 + C]$, which was helpful in identifying k^* [15]. The inset of Fig. 2 displays the position of the maximum for the 60 and 100 nm films on the patterned substrate and for that on the homogeneous section of the 100 nm film for time periods in the interval of 30 to 3060 min. For all samples, the time evolution of the characteristic

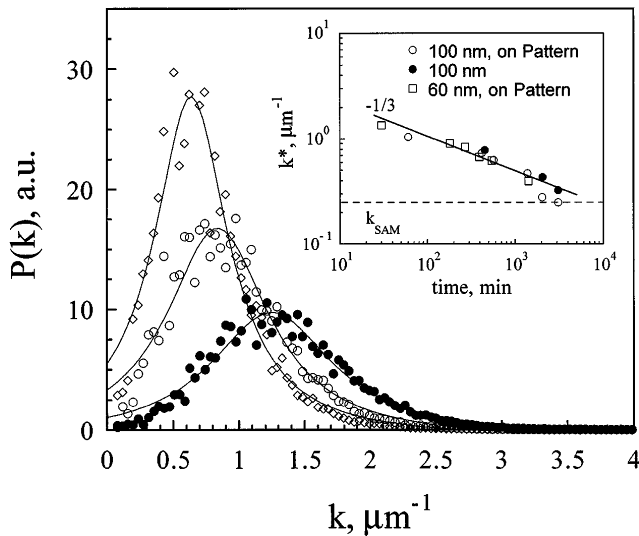

FIG. 2. Power spectra $P(k)$ obtained from radial averages of FFT data for 60 nm thick dPS/PB blend film on stripe-patterned SAM along with Lorentzian function fits to the data for three representative times: (○) 30, (●) 270, and (◇) 540 min. Inset displays position of k^* as a function of time on a log-log plot for two thicknesses (see inset legend) on the stripe-patterned area (open symbols) and on the homogeneous substrate (filled symbols) [15].

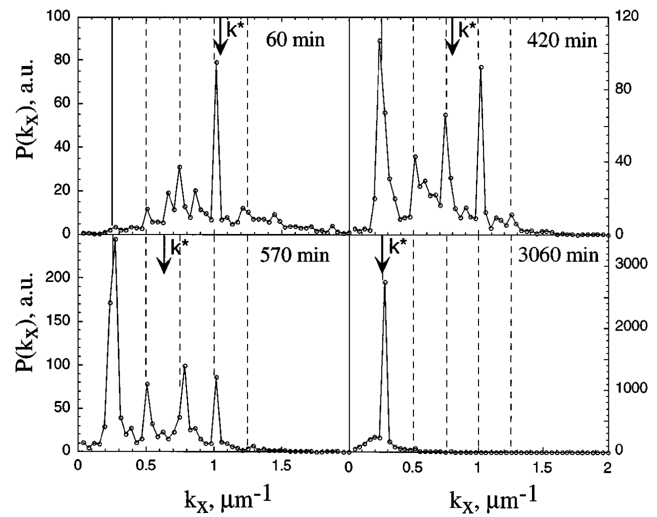

FIG. 3. Horizontal central sector power spectra [15] $P(k_x)$, obtained by averaging a narrow horizontal section of the 2D FFT transform data for 100 nm film, showing the time evolution of the harmonic peaks for four representative times. The position of the phase separation k^* (see Fig. 2) at each time interval is depicted by the arrows.

length scale $1/k^*$ is well described by a $\frac{1}{3}$ power law, independent of substrate (i.e., patterned or unpatterned) or film thickness. The $\frac{1}{3}$ scaling is representative of spinodal decomposition, Ostwald ripening, or diffusive coalescence so that it is difficult to ascribe a definite mechanism of the coarsening, beyond the statement that it reflects phase separation [12].

We next focus on the diffraction peaks which reflect the anisotropic component of the film structure. To separate this information from the isotropic intensity ring we restrict the averaging to a four pixel wide horizontal strip located in the center of the 2D FFT data array. The results of this analysis for four representative times (from 60 to 3060 min) are shown in Fig. 3, where the arrows depict the corresponding positions of k^* from Fig. 2. Several sharp peaks are evident and their positions are harmonics (i.e., $k_n = nk_1$, where n is an integer) of the first peak $k_1 = 0.25\ \mu\text{m}^{-1}$. We emphasize that the higher harmonic modes in Fig. 3 do not result from an FFT of a discontinuous topographic profile [i.e., the topography in Fig. 1(d) is not a square wave]. The value of k_1 in Figs. 3(a)–3(d) equals the inverse of the measured periodicity of the SAM pattern, i.e., $k_1 = k_{\text{SAM}}$. The positions of k_{SAM} and calculated harmonic frequencies (i.e., nk_{SAM}) are represented in Fig. 3 by vertical solid and dashed lines, respectively. While the intensities of the harmonic peaks vary with time, their positions are dictated by k_{SAM} and are therefore insensitive to the phase separation coarsening process.

The behavior described above is summarized in Fig. 4, where the intensities of the fundamental mode k_1 and the higher harmonic modes are plotted as a function of time. It can be seen in Fig. 4(b) that the intensities of the $n > 1$ modes increase at early times and decrease at long times, while the fundamental [Fig. 4(a)] increases

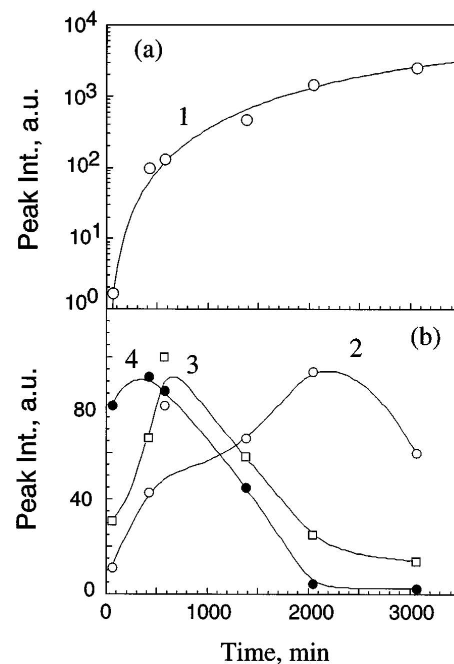

FIG. 4. Time evolution of the (a) fundamental, k_1, and (b) harmonic mode intensities. The solid line in (a) is a fit to the data using $P_1(t) = P_{\infty,1}[1 - \exp(-t/\tau)^\beta]$, where $P_{\infty,1}$ is the limiting peak intensity of the fundamental, $\beta = 2.3$, and τ is the characteristic time constant for the ordering process. The solid lines in (b) are guides to the eye.

monotonically. Figure 3 indicates that the intensity for the higher modes reaches a maximum when k^* (depicted by arrows in Fig. 3) coincides with k_n and then decreases as k^* becomes smaller. Similar results are observed on both the 60 and 100 nm films.

These observations indicate a coupling of the surface deformation and phase separation processes. The theory of shallow fluid channels [9] indicates that the free surface excitations of the boundary shape are quantized, similar to the normal modes of a vibrating string or membrane. For a rectangular channel these deformation modes should have reciprocal wavelengths k_i which are linear multiples of the fundamental frequency. In the present study the "channels" should be identified with the coexisting phases segregated to the individual SAM pattern stripes. We interpret the data in Fig. 4 as implying that the phase separation process excites the surface deformation modes when the scale of the phase separation pattern k^* becomes commensurate with the harmonic frequencies k_n. Remarkably, this "resonance" between phase separation and surface deformation occurs even at early times, when the characteristic size of the phase separation morphology is much smaller than the stripe pattern.

The amplitude of the fundamental mode, k_1, represents the degree of film ordering imposed by the underlying SAM stripe pattern. In order to quantify the characteristic time scale of this ordering process, the data in Fig. 4(a) are fit (solid line) to yield time constants, $\tau = 810$ min for the 60 nm film and $\tau = 2500$ min for the 100 nm film. This behavior indicates a faster ordering process and better alignment for the thinner film which may reflect the diminishing influence of the substrate on the surface morphology as film thickness increases [16].

Our observation of a coupling between phase separation and surface undulation modes has a number of important ramifications. The existence of this mode coupling may hinder the fabrication of multiphase polymer films by limiting the scales at which controlled structures can be formed. However, by driving the surface undulations with locally applied fields (temperature gradients, shear, electric fields, etc.) it may be possible to exploit the resonant interaction and also the interference between applied fields to create more complex surface patterns. The increasing complexity of polymer surface patterns combined with the drive towards miniaturization in materials science and biological applications requires consideration of the kind of fluctuation phenomena and associated mode-coupling effects found in the present study.

We are grateful to Professor J. W. Mays of the University of Alabama, Birmingham, for providing the deuterated poly(styrene) used in these measurements and to Eric J. Amis for his helpful comments.

[1] B. D. Ermi, A. Karim, and J. F. Douglas, J. Polym. Sci. Polym. Phys. Ed. **36**, 191 (1998).

[2] L. Sung, A. Karim, J. F. Douglas, and C. C. Han, Phys. Rev. Lett. **76**, 4368 (1996).

[3] A. Karim, T. M. Slawecki, S. K. Kumar, J. F. Douglas, S. K. Satija, C. C. Han, T. P. Russell, Y. Liu, R. Overney, J. Sokolov, and M. H. Rafailovich, Macromolecules **31**, 857 (1998).

[4] A. Vrij, Discuss. Faraday Soc. **42**, 23 (1966).

[5] F. Brochard and J. Daillant, Can. J. Phys. **68**, 1084 (1990).

[6] R. Xie, A. Karim, J. F. Douglas, C. C. Han, and R. A. Weiss, Phys. Rev. Lett. **81**, 1251 (1998).

[7] S. C. Glotzer, in *Annual Reviews of Computational Physics II,* edited by D. Stauffer (World Scientific, Singapore, 1995), pp. 1–46.

[8] M. Böltau, S. Walheim, J. Mlynek, G. Krausch, and U. Steiner, Nature (London) **391**, 877 (1998); A. Karim, J. F. Douglas, B. P. Lee, J. A. Rogers, R. J. Jackman, E. J. Amis, and G. M. Whitesides, Phys. Rev. E **57**, R6273 (1998).

[9] H. Lamb, *Hydrodynamics* (Dover, New York, 1983); J. W. Miles, Proc. R. Soc. London A **297**, 459 (1967).

[10] According to ISO 31-8, the term "molecular weight" has been replaced with "relative molecular mass," symbol M_r. The conventional notation, rather than the ISO notation, has been employed for this publication.

[11] A. Kumar, H. A. Biebuyck, and G. M. Whitesides, Langmuir **10**, 1498 (1994).

[12] L. Sung and C. C. Han, J. Polym. Sci. Polym. Phys. Ed. **33**, 2405 (1995).

[13] H. Gruell (private communication). Film thickness estimated from values obtained from x-ray reflectivity measurements of dPS/PB films cast under similar conditions on silicon substrates.

[14] The reference to commercial equipment or supplies does not imply its recommendation or endorsement by the National Institute of Standards and Technology.

[15] 256×256 sections of the 400×400 AFM height data arrays were fast Fourier transformed, and the radial averages of the squared amplitude were calculated to yield $P(k)$. In the case of the stripe-patterned substrates the horizontal central sector (4 pixels in width) of the FFT was excluded from the averages. Standard deviations are $\leq 4\%$; k^* was determined with a standard uncertainty of $\pm 0.01\ \mu\text{m}^{-1}$. The aforementioned statements do not include all components of uncertainty, but are sufficient for the internal laboratory comparisons made.

[16] G. Nisato, B. D. Ermi, J. F. Douglas, and A. Karim (to be published).